Strain-tunable magnetic anisotropy in monolayer $CrCl_3$, $CrBr_3$, and CrI_3

Lucas Webster* and Jia-An Yan†

Department of Physics, Astronomy, and Geosciences, Towson University, 8000 York Road, Towson, Maryland 21252, USA

(Received 8 June 2018; revised manuscript received 25 August 2018; published 8 October 2018)

Recent observation of intrinsic ferromagnetism in two-dimensional (2D) CrI_3 is associated with the large magnetic anisotropy due to strong spin-orbit coupling of I. Magnetic anisotropy energy (MAE) defines the stability of magnetization in a specific direction with respect to the crystal lattice and is an important parameter for nanoscale applications. In this work we apply the density functional theory to study the strain dependence of MAE in 2D monolayer chromium trihalides CrX_3 (with X = Cl, Br, and I). Detailed calculations of their energetics, atomic structures, and electronic structures under the influence of a biaxial strain ε have been carried out. It is found that all three compounds exhibit ferromagnetic ordering at the ground state (with $\varepsilon = 0$), and upon applying a compressive strain, phase transition to the antiferromagnetic state occurs. Unlike in $CrCl_3$ and $CrBr_3$, the electronic band gap in CrI_3 increases when a tensile strain is applied. The MAE also exhibits a strain dependence in the chromium trihalides: it increases when a compressive strain is applied in CrI_3, while an opposite trend is observed in the other two compounds. In particular, the MAE of CrI_3 can be increased by 47% with a compressive strain of $\varepsilon = 5\%$.

DOI: 10.1103/PhysRevB.98.144411

I. INTRODUCTION

One of the latest advances in the field of two-dimensional (2D) materials is the observation of intrinsic ferromagnetism in monolayers of $CrGeTe_3$ [1] and CrI_3 [2]. These systems provide an exciting platform for studying the interplay between various competing electronic and magnetic phenomena at the nanoscale when the quantum confinement condition is included. These include, for example, the magnetoelectric effect [3–6], spin-valley physics [7], and light-matter interactions under the influence of magnetic ordering [8].

Unlike in bulk magnetic materials, the long-range magnetic ordering in 2D structures is impossible without magnetic anisotropy, which is required for counteracting thermal fluctuations [9]. Therefore, magnetic anisotropy, which originates mainly from spin-orbit coupling (SOC) effects [10], becomes an important parameter when it comes to 2D magnets as it is qualitatively related to their magnetic stability. Moreover, ferromagnetic 2D materials with large magnetic anisotropy are of great interest for high-density magnetic memories and spintronic applications at the nanoscale, as in spin valves and magnetic tunnel junctions [11–13].

Strain engineering has been shown to be an effective approach to tune properties of nanomaterials by using substrate lattice mismatching [14–16]. It has been demonstrated that external strain can tune the electronic energy band gap in single-layer MoS_2 [14]. In particular, the way in which strain can affect magnetic anisotropy has been the subject of several studies involving thin films [17,18] and 2D materials from density-functional theory (DFT) calculations [19–21].

Typically, 2D crystals can sustain larger strains than their bulk counterpart [22,23]. Single-layer MoS_2 can sustain strains as large as 11% [22], and strains as large as 6% can be sustained in single-layer FeSe [15,16]. DFT calculations show that monolayer chromium trihalides are soft when compared with other 2D materials. A 2D Young's modulus of 24, 29, and 34 N/m has been reported for CrI_3, $CrBr_3$, and $CrCl_3$ respectively [24]. This is much smaller than that of graphene (340 N/m) [25], monolayer MoS_2 (180 N/m) [22], and monolayer FeSe (80 N/m) [26].

The softness of single-layer chromium trihalides implies that strain modulation of their electronic and magnetic properties can be realized in these systems. Here, we provide an extensive study on structural modification at the nanoscale resulting from biaxial strain by means of first-principles calculations. We also investigate the electronic structures, magnetism, and magnetic anisotropy of the single-layer chromium trihalides under different strains.

This paper is organized as follows. In Sec. II, the calculation details are given. In Sec. III, we discuss our results. A brief conclusion will be drawn in Sec. IV.

II. CALCULATIONAL METHODS

Our DFT calculations were performed using the projected augmented-wave method as implemented in the Vienna Ab initio Simulation Package (VASP) [27,28]. In all of these calculations we adopted the Perdew-Burke-Ernzerhof (PBE) [29] flavor for the generalized gradient exchange-correlation functional. The Brillouin zone was sampled by an $8\times8\times1$ k-point grid mesh [30], and a 500 eV plane-wave cutoff energy was used. Moreover, a 15-Å vacuum was applied along the z axis to avoid any artificial interactions between images. Relaxations were performed until the Hellmann-Feynman force on each atom became smaller than 0.002 eV/Å and

*lwebst6@students.towson.edu
†jiaanyan@gmail.com

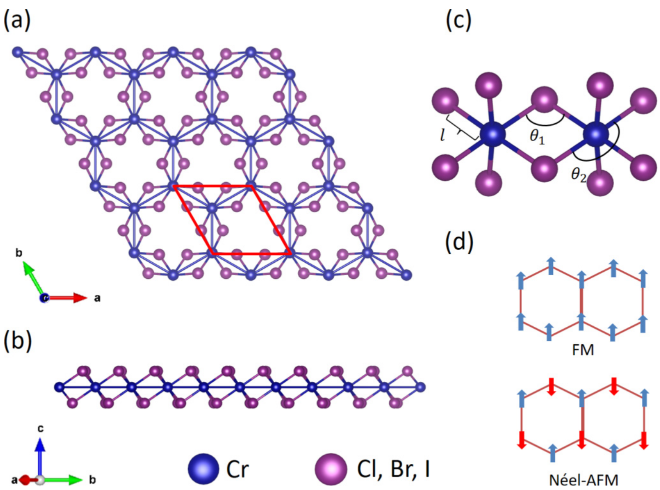

FIG. 1. Atomic structure of monolayer CrX_3 (X = Cl,Br,I). (a) Top view and (b) side view of a single layer. (c) Bonding between chromium and iodine atoms. The unit cell of CrX_3 which includes two Cr and six X atoms has been indicated in (a). The bond length l between Cr and an X atom, the bond angle θ_1 between Cr and two X atoms in the same plane, and the axial angle θ_2 are also shown in (c). (d) The two magnetic orders, namely, Néel antiferromagnetic (AFM) and ferromagnetic (FM)

the total energy was converged to be within 10^{-8} eV. Spin polarization had to be taken into account in order to reproduce the semiconducting nature of this system, and the effect of introducing SOC on the electrical and mechanical properties of these materials will be discussed. In addition, two different magnetic configurations were considered to evaluate the magnetic ground state by comparing their total energies. The ferromagnetic (FM) configuration had all magnetic moments initialized in the same direction, while in the antiferromagnetic (AFM) configuration the magnetic moments were set to be antiparallel between nearest neighbors. For both cases, spin orientations were initially in the off-plane direction. These two typical magnetic orderings are shown in Fig. 1(d).

Magnetic anisotropy energy (MAE) is defined as the difference between energies corresponding to the magnetization in the in-plane and off-plane directions (MAE $= E_{\parallel} - E_{\perp}$). Therefore, a positive (negative) value of MAE indicates the off-plane (in-plane) easy axis. To evaluate MAE, one must take SOC effects into account. Thus, noncollinear non-self-consistent calculations were performed to evaluate the total energies $E_{\parallel}$ and $E_{\perp}$ after the self-consistent ground states were achieved.

In this work, only biaxial strain has been studied. For each strain, the lattice constants were changed accordingly and then kept fixed, while the atomic positions were fully optimized. This procedure was repeated for single-layer $CrCl_3$, $CrBr_3$, and CrI_3.

III. RESULTS AND DISCUSSION

A. Atomic structures

The bulk chromium trihalides CrX_3 (X = Cl, Br, and I) are layered van der Waals materials, and the possibility of mechanically exfoliating CrI_3 to produce 2D monolayers has been demonstrated [2]. These systems exhibit rhombohedral BiI_3 structure (space group $R\bar{3}$) in cryogenic temperatures at which ferromagnetism can be observed. The Curie temperatures for the bulk systems are 27, 47, and 70 K for $CrCl_3$, $CrBr_3$, and CrI_3 respectively [31,32]. In the single-layer limit, CrI_3 retains its ferromagnetism, and the Curie temperature of the 2D system is found to be $T_c = 45$ K [2]. Figure 1(a) shows a schematic plot of the single-layer chromium trihalide compound. The chromium ions form a honeycomb network sandwiched by two atomic planes of halide atoms, as shown in Figs. 1(a) and 1(b). The parallelogram in Fig. 1(a) represents the unit cell containing two chromium atoms and six halide atoms per layer. Moreover, Cr^{3+} ions are coordinated by edge-sharing octahedra, as shown in Fig. 1(c).

Magnetism in these compounds arises from the partially filled d orbitals, as the Cr^{3+} ion has an electronic configuration of $3d^3$. Despite this fact, these materials are found to be electrical insulators, indicating that a Mott-Hubbard mechanism is playing a role in the formation of the band gap. In the octahedral environment, crystal field interaction with the halide ligands results in the quenching of orbital moment ($L = 0$) and splitting of the chromium d orbitals into a set of triply degenerate t_{2g} orbitals (with lower energy) and doubly degenerate e_g orbitals (with higher energy). Furthermore, saturation magnetization measurements give an atomic magnetic moment of $3\mu_B$ per chromium atom [33]. This is consistent with Hund's rule, which predicts that the three electrons will occupy the t_{2g} triplet yielding $S = 3/2$.

First, we investigate the structure, magnetism, and MAE of the unstrained monolayer systems. Our results from noncollinear self-consistent calculations show that the ground state for the three systems is FM, as indicated in Table I. Here, the difference in the total energy of the two magnetic phases considered in our study ($E_{\rm FM} - E_{\rm AFM}$) is less than zero for all the chromium trihalides. For this reason, only the optimized structural parameters for the FM ground state

TABLE I. The calculated lattice constants a_0, total energy E_t, bond lengths l, bond angles θ_1, and axial bond angles θ_2 for the FM phase of the chromium trihalides. The difference in energy between two magnetic phases $E_{\rm FM} - E_{\rm AFM}$, magnetic anisotropy energy (MAE), and the easy magnetization axis are also listed. SOC has been included in all calculations.

	Lattice parameters for 1-Layer					Magnetic stability for 1-Layer		
	a_0 (Å)	E_t (eV)	θ_1 (deg)	θ_2 (deg)	l (Å)	$E_{\rm FM} - E_{\rm AFM}$ (eV)	MAE (μeV/Cr)	Easy axis
$CrCl_3$	6.056	− 38.916	95.8	173.2	2.357	−0.023	24.68	c
$CrBr_3$	6.438	−35.334	95.1	173.5	2.518	−0.032	159.54	c
CrI_3	7.008	−32.318	95.2	173.3	2.740	−0.036	803.65	c

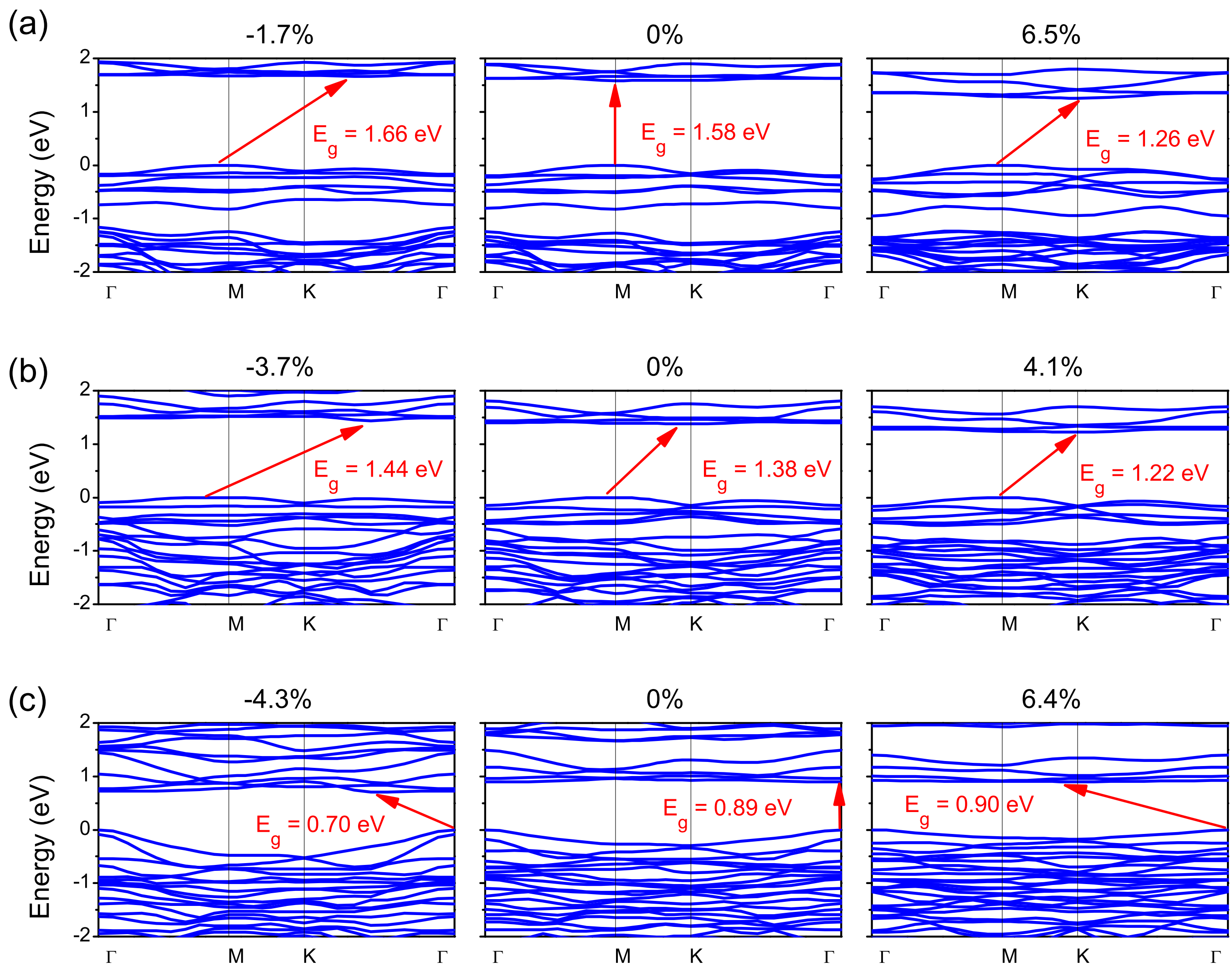

FIG. 2. Noncollinear spin-polarized electronic band dispersions for monolayer chromium trihalides. The effect of typical compressive and tensile strains is also shown for (a) $CrCl_3$, (b) $CrBr_3$, and (c) CrI_3. The energy band gaps between the conduction band minimum and valence band maximum (VBM) are indicated using red arrows in each case. The VBM has been shifted to zero.

are shown in Table I. For example, for the case of CrI_3, the lattice constant a_0 and Cr-I bond length l are 7.008 and 2.740 Å, respectively. These results are consistent with previously reported values [24,31]. The Cr-I-Cr bond angle θ_1 is 95.2° and is represented in Fig. 1(c). This angle accounts for the ferromagnetic superexchange interaction according to the Goodenough [34] and Kanamori [35] rules. The axial angle θ_2 is the angle formed between the chromium ion and two opposing ligands within the same octahedral [e.g., Fig. 1(c)]. Therefore, our results suggest some deformation in the octahedral environment as the axial angle is predicted to be slightly smaller than 180°. Interestingly, these angles are nearly independent of the ligands, as they are roughly the same for all three systems. In our previous work, we found that different magnetic orderings (FM or AFM) yield similar results for the structural parameters [36]. Moreover, these structural parameters are not sensitive to the SOC [36], which is essential for investigating the MAE below.

The calculated MAE for each compound is listed in Table I. The MAE of CrI_3 is about 804 μeV/Cr, which is surprisingly large when compared to the other compounds in Table I. Previous studies reported 980 μeV/Cr [5] and 686 μeV/Cr [24], and these discrepancies might result from the different methods adopted. Lado and Fernández-Rossier suggested that the large MAE in CrI_3 originates from an anisotropic exchange interaction through a superexchange mechanism, which stems from the strong SOC in the heavier iodine ions [10]. In addition, the easy axis for energetically favorable spontaneous magnetization is found to be perpendicular to the basal plane, i.e., along the c direction.

B. Electronic structures

The electronic band structures for $CrCl_3$, $CrBr_3$, and CrI_3 under various biaxial strains are shown in Figs. 2(a), 2(b), and 2(c), respectively. In Ref. [36], we already showed that the band structure of CrI_3 is highly sensitive to the magnetic ordering, the exchange-correlation functional, and SOC. Here, we focus on the results calculated from PBE for only the FM phase. The effect of SOC on the electronic band structure can be further elucidated by comparing Fig. 2 with Fig. S1 in the Supplemental Material [37], which shows the collinear

TABLE II. The exchange coupling and Curie temperature of single-layer chromium trihalides.

	J (meV)	Estimated T_c (K)	Experimental T_c (K)
$CrCl_3$	1.7	29.7	27 (bulk) [31]
$CrBr_3$	2.4	41.3	47 (bulk) [31]
CrI_3	2.7	46.4	70 (bulk) [31], 45 (1-Layer) [2]

results. Unlike CrI_3, the band structures of the other compounds are insensitive to the inclusion of SOC. This provides further evidence that MAE in these systems is closely related to the SOC in the halide ligands.

Clearly, the band gaps increase from 0.89 to 1.58 eV from iodine to chlorine. Both $CrCl_3$ and CrI_3 exhibit a direct band gap. The band gap character found for unstrained CrI_3 is consistent with previous works, which also included SOC [5,26]. In addition, from Figs. 2(a) and 2(b), we notice an increase (decrease) in the band gap upon compression (tensile strain) in these systems. However, according to Fig. 2(c), the application of a biaxial strain causes an opposite effect on the band gap of CrI_3. In the three compounds, the valence band maximum remains approximately constant with the application of strain, whereas the conduction band minimum is shifted, causing a direct-to-indirect band gap transition in both $CrCl_3$ and CrI_3. Moreover, a compressive strain will decrease the energy of the valence bands near the M and K points in CrI_3. This effect can also be observed in collinear calculations; however, it is more evident when SOC is included.

C. Effect of strain on crystal structure and the magnetic order

Next, we investigate the dependence of magnetic properties under different strains. It is mainly Cr atoms that contribute to the magnetic moment, which remains overall constant with $6\mu_B$ (two Cr^{3+} ions per unit cell) per unit cell under strain (not shown). Figure 3 shows the energy difference between the two magnetic orderings, namely, FM and AFM. A phase transition from FM to AFM is observed in all systems, and the AFM region is highlighted in red. Here, the strain ε is defined as

$$\varepsilon = \frac{(a - a_0)}{a_0}, \tag{1}$$

where a_0 is the lattice constant for the unstrained system. The energy difference of the two phases is given by (neglecting the MAE since it is relatively small) [24]

$$E_{\mathrm{FM/AFM}} = E_0 - (\pm 3J_1 + 6J_2 \pm 3J_3)|\vec{S}|^2, \tag{2}$$

where J_1, J_2, and J_3 are the Heisenberg exchange integrations for the first-, second-, and third-nearest neighbors, respectively. Neglecting the second- and third-nearest neighbors and taking the energy difference between FM and AFM phases, we have

$$E_{\mathrm{FM}} - E_{\mathrm{AFM}} = -6J|\vec{S}|^2. \tag{3}$$

Here, $|\vec{S}| = 3/2$. From the energy difference calculated in DFT (as shown in Table I), one can determine the exchange parameter J with Eq. (3). Next, with J available one can roughly estimate the Curie temperature from the mean-field expression:

$$T_c = \frac{3J}{2K_B}. \tag{4}$$

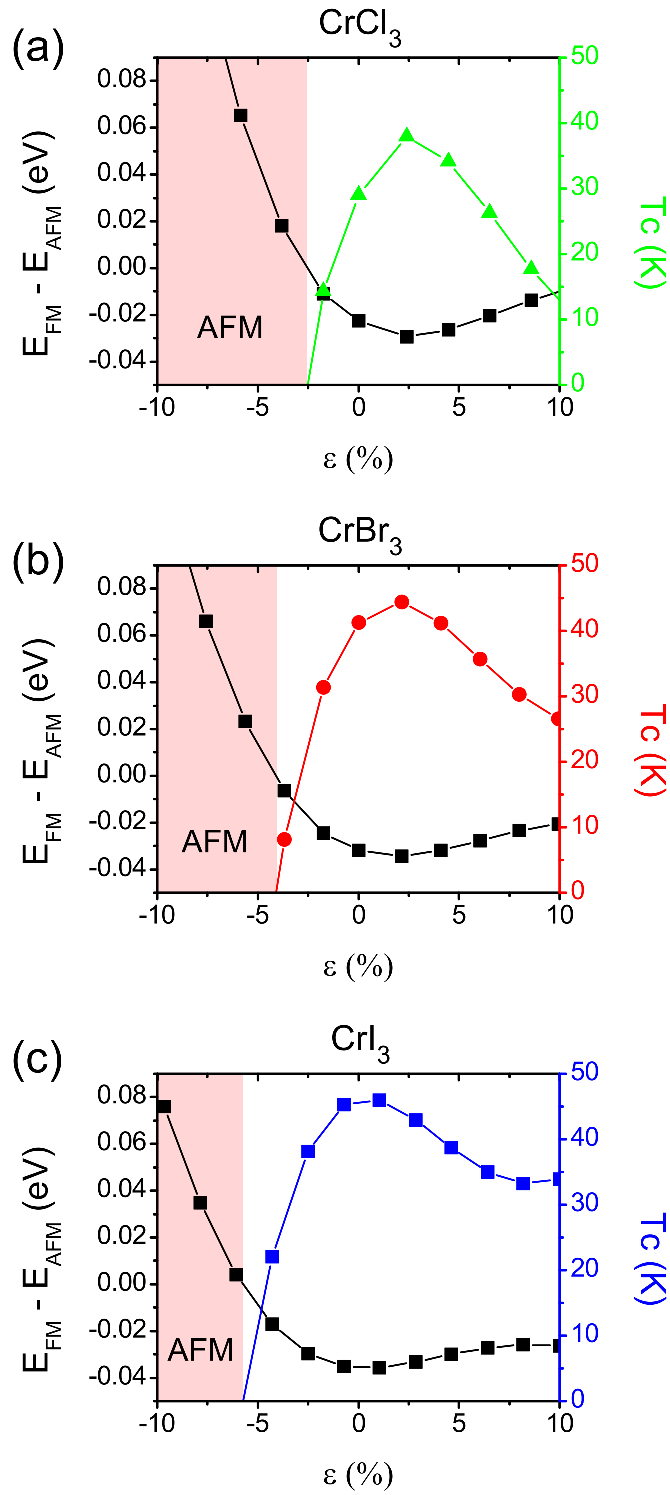

FIG. 3. Energy difference between the FM and AFM phases for (a) $CrCl_3$, (b) $CrBr_3$, and (c) CrI_3. The AFM phase region is highlighted in red. The calculated Curie temperature is also shown for each case.

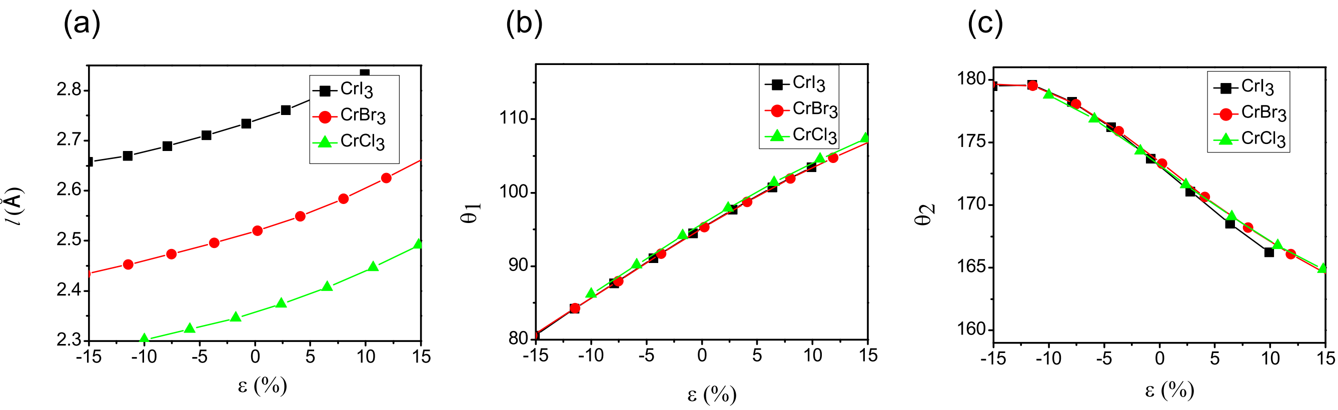

FIG. 4. Dependence of structural parameters on biaxial strain ε for the chromium trihalides. (a) Bond length l. (b) Bond angle θ_1. (c) Axial bond angle θ_2.

A brief derivation is provided in the Supplemental Material [37]. The Heisenberg exchange parameter and the estimated Curie temperature for the unstrained systems are listed in Table II, along with the available experimental values for the Curie temperature. The obtained value for J, considering only the first-nearest neighbors, agrees with previous DFT calculations [24]. From Table II, the estimated Curie temperatures for single-layer $CrCl_3$ and $CrBr_3$ are approximately equal to the experimental values for the bulk systems. Whereas there is a difference between the Curie temperatures for the bulk CrI_3 and monolayer CrI_3, our estimation is closer to that of monolayer CrI_3. This is expected since Eq. (4) is valid for the 2D system and suggests a relatively large interlayer coupling in bulk CrI_3.

In Fig. 3, we show the energy difference $E_{FM} - E_{AFM}$ between the two magnetic orderings as a function of ε for $CrCl_3$, $CrBr_3$, and CrI_3. The evolution of the Curie temperature calculated based on Eq. (4) is also shown in Fig. 3 (right axis). As ε decreases (i.e., the compressive strain increases), the energy difference increases. There is a phase transition to the AFM phase when the energy difference between FM and AFM orderings becomes greater than zero. This phase transition occurs at -2.5%, -4.1%, and -5.7% compressive strain for $CrCl_3$, $CrBr_3$, and CrI_3, respectively. A similar result was reported by Zheng *et al.* for CrI_3 under compressive strain [26]. According to Fig. 3, there is a point at which the Curie temperature is maximum, and this point is close to the equilibrium for CrI_3. However, as shown in Fig. 3(a), this point is slightly shifted from the equilibrium to the region with small tensile strain in $CrCl_3$ and $CrBr_3$, suggesting that in these cases the Curie temperature can be further increased with the introduction of tensile strain. We estimate that a tensile strain of 2.4% can increase T_c to 39.0 K in $CrCl_3$, and a tensile strain of 2.1% can increase T_c to 44.4 K in $CrBr_3$. Beyond this point of local maximum, the Curie temperature tends to decrease, and no transition to the AFM phase is observed if we further increase tensile strain within the 10% range.

We have also calculated the effect of strain on the structural parameters, as depicted in Fig. 4. These calculations were repeated for each material with different magnetic orderings (FM and AFM). Since results of AFM are similar, we show only the results for the FM phase. From Fig. 4, one can clearly see that the Cr-X-Cr angle changes linearly with respect to strain. In addition, the angle with $\varepsilon = 0$ is roughly the same (95°) for the three halides. Within the 10% range from the equilibrium point ($\varepsilon = 0$), the curves display a linear shape with the same slope for the three materials. The axial angle has a similar behavior but tends to increase upon compression until it saturates near 180°. At this point, with the axial angle fully stretched (around -10% of compression for all materials), the system achieves a higher degree of symmetry. The Cr-X distance displays a weak strain dependency within the 10% range.

D. Effect of strain on the magnetic anisotropy energy

One can also observe how MAE changes with biaxial strain in Fig. 5. In Figs. 5(a)–5(c), the energy was calculated as a function of the angle of magnetization with respect to the basal plane θ_M, which is 0° in plane and 90° off plane. This is illustrated in the inset of Fig. 5(f), where $E_\parallel$ and $E_\perp$ represent the energies calculated when all the spins are parallel and perpendicular to the atomic plane, respectively. These calculations were repeated for different values of strain. If we neglect the higher-order terms, the dependency of the energy per chromium atom with respect to θ_M is given by [38]

$$E(\theta_M) = E_0 + \lambda_1 \sin^2(\theta_M) + \lambda_2 \sin^4(\theta_M). \quad (5)$$

Here, E_0 is a constant-energy shift, and λ_1 and λ_2 are, respectively, the quadratic and quartic contributions to the energy. No substantial difference in energy with respect to the different in-plane directions is observed from DFT calculations; therefore, the azimuthal contribution to $E(\theta_M)$ is neglected. From Figs. 5(a)–5(c) we note that $E(\theta_M)$ provides a good fit for the energies. In addition, it can be seen from Figs. 5(a)–5(c) that the easy axis remains off plane for CrI_3 and $CrBr_3$ even when subject to strain, whereas for $CrCl_3$ there exists a phase transition to an in-plane easy axis upon compression. This can be further verified by looking at Figs. 5(d)–5(f), in which we take the difference between in-plane ($E_\parallel$) and off-plane ($E_\perp$) energies and plot them with respect to strain. Here, negative values seen in Fig. 5(d) for $CrCl_3$ represent an in-plane preference for magnetization.

Although bulk $CrCl_3$ is found to possess an in-plane easy axis [39], it should be noted from Fig. 5(d) that the MAE

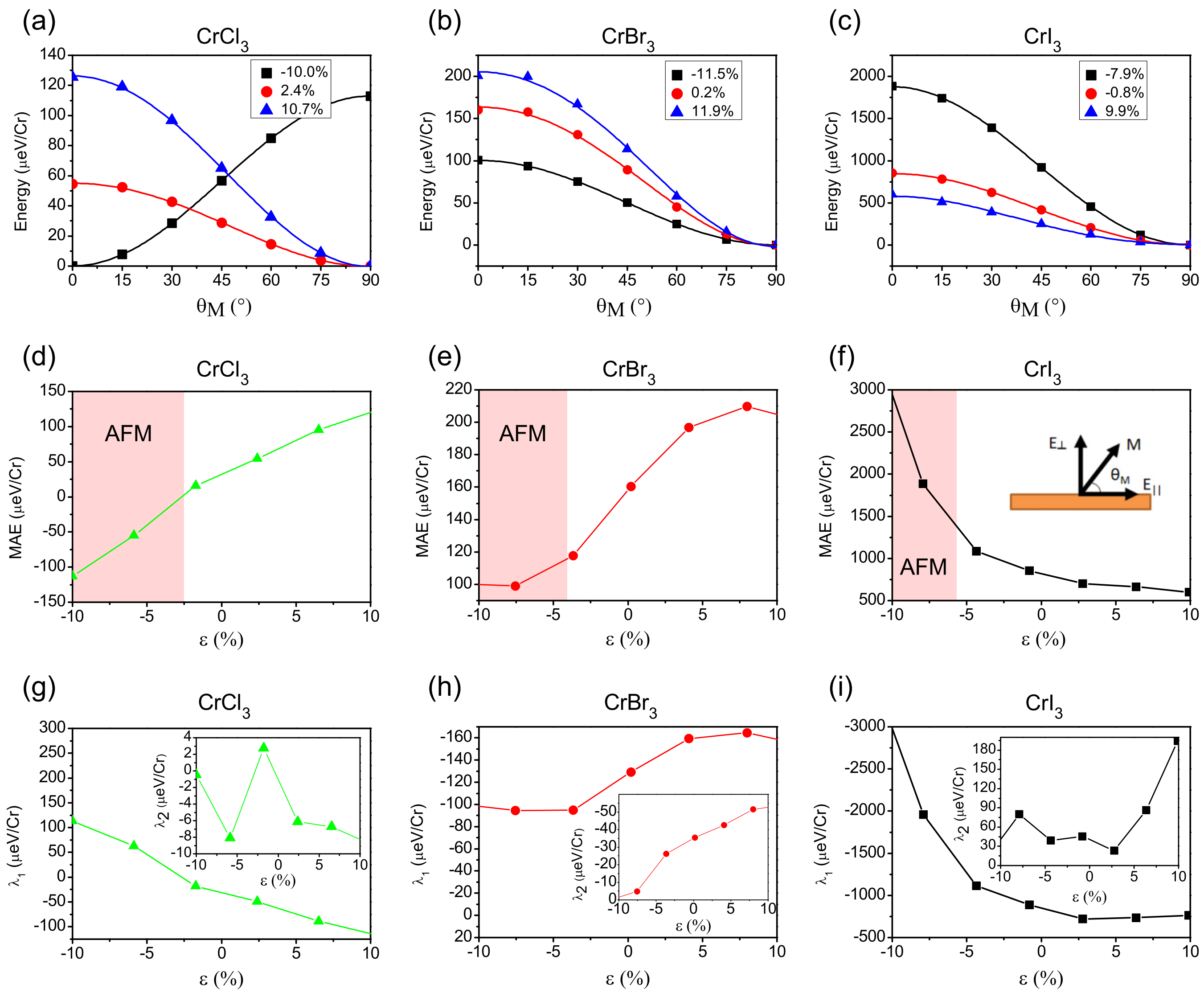

FIG. 5. The effect of strain on the magnetic anisotropic energy. Change in energy with respect to the magnetization angle θ_M for (a) $CrCl_3$, (b) $CrBr_3$, and (c) CrI_3. The lines are the fitted results. Change in MAE with respect to strain in (d) $CrCl_3$, (e) $CrBr_3$, and (f) CrI_3. The AFM phase region is highlighted in red. (g)–(i) The change in the fitted parameters λ_1 and λ_2.

of unstrained monolayer $CrCl_3$ is positive, indicating that the spins of Cr atoms align perpendicular to the basal plane, even though the MAE is much smaller than that of CrI_3. A similar result was also reported by Zhang *et al.* [24]. This result suggests a possible transition from an in-plane to an off-plane easy axis for $CrCl_3$ upon exfoliation. This is not surprising, considering that the MAE of $CrCl_3$ is much smaller than that of CrI_3. Furthermore, unlike the $CrBr_3$ and $CrCl_3$ compounds, the CrI_3 crystal exhibits much stronger anisotropy when compressed and becomes weaker when stretched. More specifically, a −5% compressive strain will increase the MAE by 47% in this system.

Fitting parameters for λ_1 and λ_2 can be found in Figs. 5(g)–5(i). These plots show the strain dependence of these constants for the three monolayer systems, with the λ_2 graph being displayed in the inset. We note that for all systems the quadratic contribution dominates the MAE, as the change in λ_1 resembles the MAE curves for each compound. However, as tensile strain increases, the quartic contribution becomes comparable to the quadratic contribution in magnitude for $CrBr_3$ and CrI_3.

Finally, we would like to point out that calculations based on the local-density approximation yield similar effects on strain on the MAE, although the value is slightly different [see Fig. S3(a) in the Supplemental Material]. In addition, the MAE is strongly dependent on the on-site parameter of Hubbard U for Cr. Our PBE+U calculations show that the MAE increases dramatically when the Hubbard U parameter is increased. The enhancement in the MAE with respect to a 5% compressive strain ranges from 20.7% to 58.1% depending on the value of the Hubbard U parameter. All the data are included in the Supplemental Material [37].

IV. CONCLUSIONS

In summary, we applied density functional theory to investigate the magnetic and electronic properties of a recently found 2D magnet, monolayer CrI_3, and other compounds from the same family, including $CrBr_3$ and $CrCl_3$. All three monolayer systems are found to be ferromagnetic in the ground state in accordance with previous work. In addition, CrI_3 exhibits strong magnetic anisotropy (804 μeV/Cr) with an easy axis perpendicular to the basal plane. The MAE decreases dramatically as the atomic number of the halide decreases, with $CrBr_3$ and $CrCl_3$ having 160 and 25 μeV/Cr, respectively. We also estimated the Curie temperature from mean-field approximation and the calculated energy differences between two different magnetic orders, namely, FM and AFM. Our results are in good agreement with experimental data and suggest a relatively large interlayer coupling in the CrI_3 system. Interestingly, our mean-field estimation predicts that the Curie temperature for $CrCl_3$ can increase from 29.7 to 39 K with 2.4% tensile strain.

Furthermore, we have studied the effect of biaxial strain and have determined the strain dependence of the atomic structure and electronic and magnetic properties of the chromium trihalides. Strong SOC in the CrI_3 results in a more evident strain dependence of the electronic and magnetic properties than in $CrBr_3$ and $CrCl_3$. For example, the MAE in CrI_3 increases when compressed and decreases when stretched. A 5% compressive strain will increase MAE by 47% in this system.

ACKNOWLEDGMENTS

This work used the Extreme Science and Engineering Discovery Environment (XSEDE) Comet at the SDSC through allocations TG-DMR160101 and TG-DMR16088. We acknowledge support from NSF Grant No. DMR 1709781 and support from the Fisher General Endowment and SET grants from the Jess and Mildred Fisher College of Science and Mathematics at Towson University.

[1] C. Gong, L. Li, Z. Li, H. Ji, A. Stern, Y. Xia, T. Cao, W. Bao, C. Wang, Y. Wang *et al.*, Discovery of intrinsic ferromagnetism in two-dimensional van der Waals crystals, Nature (London) **546**, 265 (2017).

[2] B. Huang, G. Clark, E. Navarro-Moratalla, D. R. Klein, R. Cheng, K. L. Seyler, D. Zhong, E. Schmidgall, M. A. McGuire, D. H. Cobden *et al.*, Layer-dependent ferromagnetism in a van der Waals crystal down to the monolayer limit, Nature (London) **546**, 270 (2017).

[3] B. Huang, G. Clark, D. R. Klein, D. MacNeill, E. Navarro-Moratalla, K. L. Seyler, N. Wilson, M. A. McGuire, D. H. Cobden, D. Xiao *et al.*, Electrical control of 2D magnetism in bilayer CrI_3, Nat. Nanotechnol. **13**, 544 (2018).

[4] S. Jiang, J. Shan, and K. F. Mak, Electric-field switching of two-dimensional van der Waals magnets, Nat. Mater. **17**, 406 (2018).

[5] P. Jiang, L. Li, Z. Liao, Y. X. Zhao, and Z. Zhong, Spin direction-controlled electronic band structure in two-dimensional ferromagnetic CrI_3, Nano Lett. **18**, 3844 (2018).

[6] S. Jiang, L. Li, Z. Wang, K. F. Mak, and J. Shan, Controlling magnetism in 2D CrI_3 by electrostatic doping, Nat. Nanotechnol. **13**, 549 (2018).

[7] D. Zhong, K. L. Seyler, X. Linpeng, R. Cheng, N. Sivadas, B. Huang, E. Schmidgall, T. Taniguchi, K. Watanabe, M. A. McGuire *et al.*, van der Waals engineering of ferromagnetic semiconductor heterostructures for spin and valleytronics, Sci. Adv. **3**, e1603113 (2017).

[8] K. L. Seyler, D. Zhong, D. R. Klein, S. Gao, X. Zhang, B. Huang, E. Navarro-Moratalla, L. Yang, D. H. Cobden, M. A. McGuire *et al.*, Ligand-field helical luminescence in a 2D ferromagnetic insulator, Nat. Phys. **14**, 277 (2018).

[9] N. D. Mermin and H. Wagner, Absence of Ferromagnetism or Antiferromagnetism in One- or Two-Dimensional Isotropic Heisenberg Models, Phys. Rev. Lett. **17**, 1133 (1966).

[10] J. L. Lado and J. Fernández-Rossier, On the origin of magnetic anisotropy in two dimensional CrI_3, 2D Mater. **4**, 035002 (2017).

[11] B. A. Gurney, M. Carey, C. Tsang, M. Williams, S. S. P. Parkin, R. E. Fontana, E. Grochowski, M. Pinarbasi, T. Lin, and D. Mauri, Spin valve giant magnetoresistive sensor materials for hard disk drives, in *Ultrathin Magnetic Structures IV* (Springer, Berlin, 2005), pp. 149–175.

[12] M. H. Kryder, Magnetic thin films for data storage, Thin Solid Films **216**, 174 (1992).

[13] G. A. Prinz, Magnetoelectronics, Science **282**, 1660 (1998).

[14] H. J. Conley, B. Wang, J. I. Ziegler, R. F. Haglund, Jr., S. T. Pantelides, and K. I. Bolotin, Bandgap engineering of strained monolayer and bilayer MoS_2, Nano Lett. **13**, 3626 (2013).

[15] P. Zhang, X. L. Peng, T. Qian, P. Richard, X. Shi, J. Z. Ma, B. B. Fu, Y. L. Guo, Z. Q. Han, S. C. Wang *et al.*, Observation of high-T_c superconductivity in rectangular FeSe/$SrTiO_3$ (110) monolayers, Phys. Rev. B **94**, 104510 (2016).

[16] R. Peng, H. C. Xu, S. Y. Tan, H. Y. Cao, M. Xia, X. P. Shen, Z. C. Huang, C. H. P. Wen, Q. Song, T. Zhang *et al.*, Tuning the band structure and superconductivity in single-layer FeSe by interface engineering, Nat. Commun. **5**, 5044 (2014).

[17] J. A. Heuver, A. Scaramucci, Y. Blickenstorfer, S. Matzen, N. A. Spaldin, C. Ederer, and B. Noheda, Strain-induced magnetic anisotropy in epitaxial thin films of the spinel $CoCr_2O_4$, Phys. Rev. B **92**, 214429 (2015).

[18] A. Rajapitamahuni, L. Zhang, M. A. Koten, V. R. Singh, J. D. Burton, E. Y. Tsymbal, J. E. Shield, and X. Hong, Giant Enhancement of Magnetic Anisotropy in Ultrathin Manganite Films via Nanoscale 1D Periodic Depth Modulation, Phys. Rev. Lett. **116**, 187201 (2016).

[19] W. Zhang, H. T. Guo, J. Jiang, Q. C. Tao, X. J. Song, H. Li, and J. Huang, Magnetism and magnetocrystalline anisotropy in single-layer $PtSe_2$: Interplay between strain and vacancy, J. Appl. Phys. **120**, 013904 (2016).

[20] H. L. Zhuang, P. R. C. Kent, and R. G. Hennig, Strong anisotropy and magnetostriction in the two-dimensional stoner ferromagnet Fe_3GeTe_2, Phys. Rev. B **93**, 134407 (2016).

[21] J. Zhang, B. Yang, H. Zheng, X. Han, and Y. Yan, Large magnetic anisotropy and strain induced enhancement of magnetic anisotropy in monolayer $TaTe_2$, Phys. Chem. Chem. Phys. **19**, 24341 (2017).

[22] S. Bertolazzi, J. Brivio, and A. Kis, Stretching and breaking of ultrathin MoS_2, ACS Nano **5**, 9703 (2011).

[23] K. S. Kim, Y. Zhao, H. Jang, S. Y. Lee, J. M. Kim, K. S. Kim, J. H. Ahn, P. Kim, J. Y. Choi, and B. H. Hong, Large-scale pattern growth of graphene films for stretchable transparent electrodes, Nature (London) **457**, 706 (2009).

[24] W. B. Zhang, Q. Qu, P. Zhu, and C. H. Lam, Robust intrinsic ferromagnetism and half semiconductivity in stable two-dimensional single-layer chromium trihalides, J. Mater. Chem. C **3**, 12457 (2015).

[25] A. Politano and G. Chiarello, Probing the young's modulus and poisson's ratio in graphene/metal interfaces and graphite: A comparative study, Nano Res. **8**, 1847 (2015).

[26] F. Zheng, J. Zhao, Z. Liu, M. Li, M. Zhou, S. Zhang, and P. Zhang, Tunable spin states in the two-dimensional magnet CrI_3, Nanoscale **10**, 14298 (2018).

[27] G. Kresse and D. Joubert, From ultrasoft pseudopotentials to the projector augmented-wave method, Phys. Rev. B **59**, 1758 (1999).

[28] G. Kresse and J. Furthmüller, Efficient iterative schemes for *ab Initio* total-energy calculations using a plane-wave basis set, Phys. Rev. B **54**, 11169 (1996).

[29] J. P. Perdew, K. Burke, and M. Ernzerhof, Generalized Gradient Approximation Made Simple, Phys. Rev. Lett. **77**, 3865 (1996).

[30] H. J. Monkhorst and J. D. Pack, Special points for brillouin-zone integrations, Phys. Rev. B **13**, 5188 (1976).

[31] M. A. McGuire, H. Dixit, V. R. Cooper, and B. C. Sales, Coupling of crystal structure and magnetism in the layered, ferromagnetic insulator CrI_3, Chem. Mater. **27**, 612 (2015).

[32] M. McGuire, Crystal and magnetic structures in layered, transition metal dihalides and trihalides, Crystals **7**, 121 (2017).

[33] N. Richter, D. Weber, F. Martin, N. Singh, U. Schwingenschlögl, B. V. Lotsch, and M. Kläui, Temperature-dependent magnetic anisotropy in the layered magnetic semiconductors CrI_3 and $CrBr_3$, Phys. Rev. Mater. **2**, 024004 (2018).

[34] J. B. Goodenough, An interpretation of the magnetic properties of the perovskite-type mixed crystals $La_{1-x}Sr_xCoO_{3-\lambda}$, J. Phys. Chem. Solids **6**, 287 (1958).

[35] J. Kanamori, Superexchange interaction and symmetry properties of electron orbitals, J. Phys. Chem. Solids **10**, 87 (1959).

[36] L. Webster, L. Liang, and J. A. Yan, Distinct spin-lattice and spin-phonon interactions in monolayer magnetic CrI_3, Phys. Chem. Chem. Phys. **20**, 23546 (2018).

[37] See Supplemental Material at http://link.aps.org/supplemental/10.1103/PhysRevB.98.144411 for collinear band structure calculations, a brief derivation of the equation used to estimate the Curie temperature, and for MAE versus strain curves generated from local-density approximation and PBE+U calculations.

[38] A. N. Bogdanov and I. E. Dragunov, Metastable states, spin-reorientation transitions, and domain structures in planar hexagonal antiferromagnets, Low Temp. Phys. **24**, 852 (1998).

[39] M. A. McGuire, G. Clark, K. C. Santosh, W. M. Chance, G. E. Jellison, Jr., V. R. Cooper, X. Xu, and B. C. Sales, Magnetic behavior and spin-lattice coupling in cleavable van der Waals layered $CrCl_3$ Crystals, Phys. Rev. Mater. **1**, 014001 (2017).